Topological Chiral Magnons in the Altermagnet AgF_2 Monolayer

J. W. González[1*], R. A. Gallardo[2], N. Vidal-Silva[3], and A. M. León[4*]

[1]*Departamento de Física, Universidad de Antofagasta, Av. Angamos 601, Casilla 170, Antofagasta, Chile*
[2] *Departamento de Física, Universidad Técnica Federico Santa María, Casilla Postal 110V, Valparaíso, Chile*
[3]*Departamento de Ciencias Físicas, Universidad de La Frontera, Casilla 54-D, Temuco, Chile*
[4]*Departamento de Física, Facultad de Ciencias, Universidad de Chile, Casilla 653, Santiago, Chile*

(Received 24 October 2025; accepted manuscript online 23 December 2025)

Altermagnets have emerged as a fertile ground for quantum phenomena, but topological phases unifying different quasiparticles remain largely unexplored. Here, we demonstrate that monolayer AgF_2 hosts a dual topological state, driven by a single ferroelastic distortion. This polar transition breaks inversion symmetry and unleashes relativistic spin–orbit effects, simultaneously imparting non-trivial topology to electrons and magnons. The result is valence bands with opposite Chern numbers, $C^{\mathrm{E}} = \pm 3$, and a magnon spectrum with a full topological gap and chiral bands, $C^{\mathrm{M}} = \pm 1$. This work realizes topological altermagnonics in a tangible material platform, with a clear experimental fingerprint in the transverse thermal Hall effect. The coexistence of fermionic and bosonic topology in AgF_2 opens new directions for designing intrinsically hybrid quantum matter.

DOI: 10.1088/0256-307X/43/2/020705 CSTR: 32039.14.0256-307X.43.2.020705

1. Introduction. Topological phases of matter, first identified in electronic systems, have recently been extended to bosonic quasiparticles such as magnons, the quantized spin waves in magnetic insulators.[1–4] While their study has been fruitful in ferromagnets, realizing such features in conventional collinear antiferromagnets (AFMs) is challenging, as their magnon branches are typically degenerate due to high crystal symmetry.[5] Altermagnetism (AM), a newly recognized class of collinearly compensated magnets, circumvents this challenge via a unique rotational symmetry that intrinsically lifts the magnon degeneracy, providing an ideal platform for realizing topological phases.[6–9] Within the recently established parity framework of unconventional magnets,[10] altermagnets belong to the even-parity class, where spin splitting is symmetric under momentum inversion, $\Delta E(\boldsymbol{k}) = \Delta E(-\boldsymbol{k})$.[6] This contrasts with odd-parity p-wave magnets, which arise from non-collinear spin textures and feature $\Delta E(\boldsymbol{k}) = -\Delta E(-\boldsymbol{k})$.[11,12] This classification is essential for contextualizing how relativistic interactions can hybridize odd- and even-parity characteristics, a mechanism we uncover in monolayer AgF_2.[13]

Silver fluorides, particularly AgF_2, represent a compelling frontier in correlated electron systems because they are the closest known analogs of the cuprates.[14,15] This has fueled extensive theoretical predictions of unconventional d-wave superconductivity upon doping,[16] akin to their cuprate counterparts. Yet this scenario faces severe experimental hurdles: superconductivity in AgF_2 remains elusive, as carrier doping is strongly frustrated by phase separation and polaronic self-trapping.[15,17] More recently, the discovery of AM has opened an entirely different pathway. Theory now predicts that altermagnets can host unconventional spin-triplet (p-wave or f-wave) and even topological superconductivity,[18] a mechanism distinct from the cuprate paradigm. Our work lies at the intersection of these two routes. We demonstrate that monolayer AgF_2 stabilizes a polar altermagnetic ground state, a phase where the key ingredients for both scenarios coexist. Crucially, we show that this state is not a passive starting point but a distinct form of emergent quantum matter: a dual topological phase with intrinsically coupled electronic and magnonic orders.

In this work, we identify AgF_2 as a compelling candidate in which a structural distortion drives the system from a centrosymmetric, topologically trivial AFM to a polar, ferroelastic altermagnetic ground state.[19] This transition not only activates a non-relativistic altermagnetic spin splitting but, upon inclusion of spin–orbit coupling (SOC), also stabilizes a striking electronic topological phase where the two highest valence bands carry opposite Chern numbers, $C^{\mathrm{E}} = \pm 3$. In parallel, the same distortion enhances magnetic interactions, generating a robust Dzyaloshinskii–Moriya (DM) term that opens a full topological gap in the magnon spectrum and yields non-degenerate bands with $C^{\mathrm{M}} = \pm 1$.[4] These topological magnons constitute a direct realization of altermagnonics, giving rise to a finite transverse thermal Hall conductivity that provides a clear experimental hallmark. Our results, therefore, unveil an unprecedented platform where a single structural switch entangles electronic and magnonic topology, charting a route toward multifunctional quantum materials that intrinsically couple fermionic and bosonic quasiparticles.

Our findings establish monolayer AgF_2 as a unique

*Corresponding authors. Email: jhon.gonzalez@uantof.cl; andrea.leon@iuchile.cl
© 2026 Chinese Physical Society and IOP Publishing Ltd. All rights, including for text and data mining, AI training, and similar technologies, are reserved.

platform where a single, symmetry-lowering mechanism imparts non-trivial topology to both electronic and magnonic excitations. This discovery introduces a symmetry-based route to engineer coupled fermionic and bosonic topological transport in collinear magnets. More broadly, our results suggest that planar two-dimensional transition-metal halides,[20,21] MX_2 (M = transition metal; X = halide), constitute a versatile class of quantum materials where structural distortions and relativistic interactions conspire to generate topological phases across multiple quasiparticle sectors. Taken together, these insights establish 2D halide magnets as a unifying platform where intertwined topological fermions and bosons may emerge as a generic feature, opening avenues toward device concepts that harness electron–magnon interconversion and hybrid quantum transport.

2. Methodology. We perform first-principles calculations with the Vienna *ab initio* simulation package (VASP)[22] using the projector augmented-wave method.[23] Exchange-correlation effects are described within the generalized gradient approximation in the Perdew–Burke–Ernzerhof parametrization.[24] We use a kinetic-energy cutoff of 450 eV for the plane-wave basis set, above the recommended values of the employed PAW pseudopotentials. To extract the magnetic exchange coupling constants, additional calculations are performed within a localized basis-set density functional theory (DFT) framework using the OpenMX package[25,26] within equivalent parameters.

We model the AgF_2 monolayer in a slab geometry with a vacuum region of at least 15 Å along the out-of-plane direction to prevent spurious interlayer interactions. The Brillouin zone is sampled with Monkhorst-Pack meshes of $10\times9\times1$ for structural relaxations and $20\times18\times1$ for static self-consistent calculations, corresponding to k-point spacings of approximately 0.02 and 0.01 $2\pi/$Å, respectively.[27] We use Methfessel–Paxton smearing with a width of 0.05 eV during ionic relaxations. Atomic positions are relaxed until the residual forces on each atom are smaller than 10^{-3} eV/Å, with electronic self-consistency reached within 10^{-6} eV. To account for strong on-site Coulomb interactions of Ag 4d states, we apply the rotationally invariant DFT+U approach in the Dudarev formalism,[28] with an effective parameter $U_{\text{eff}} = 4$ eV. This choice, consistent with earlier studies of Ag(II) fluorides,[14,29] reproduces key experimental observables such as the insulating band gap and the magnitude of local magnetic moments in AgF_2.

3. Electronic Properties. The physical properties of monolayer AgF_2 are intrinsically linked to its crystal structure. This work studies two key structural polymorphs, depicted in Fig. 1: (a) a high-symmetry, flat geometry and (b) a distorted, tilted ground-state geometry. These structures differ fundamentally in their point group symmetry, fluorine atom arrangement, and, most critically, their inversion properties. The subsequent sections demonstrate how these crystallographic distinctions give rise to profoundly different electronic and magnetic behaviors, establishing a direct connection between the crystal geometry and the emergent topological phenomena. Throughout this work, all electronic band structures are referenced to the Fermi energy, which is set to zero ($E_{\text{F}} = 0$).

3.1. Geometry: From centrosymmetric AFM to polar AM. The flat polymorph, shown in Fig. 1(a), provides a high-symmetry structural reference. It possesses a tetragonal lattice described by the centrosymmetric, non-polar space group $P4/mmm$ (No. 123), with all atoms confined to a single plane. The AgF_4 square motifs are perfectly flat and undistorted. Consequently, the two Ag sublattices are crystallographically equivalent, related by an inversion center. Our DFT calculations confirm this phase is metastable, with a magnetic moment of $0.453\,\mu_{\text{B}}$ lies approximately 0.2 eV per formula unit above the ground state. In this configuration, the inversion symmetry connects the two Ag sites. In contrast, the actual structural ground state, depicted in Fig. 1(b), adopts the polar monoclinic space group $P2_1$ (No. 4). Here, the lattice undergoes a cooperative distortion involving the tilting and buckling of the AgF_4 units, which breaks both the fourfold rotational and, most critically, the inversion symmetries. The resulting relaxed unit cell is anisotropic, with a calculated in-plane aspect ratio of $a/b \approx 0.87$ and a magnetic moment of $0.528\,\mu_B$. This distortion is quantified by three primary parameters: an out-of-plane tilt $|\theta| = 24.1°$, an in-plane rotation $|\varphi_{21}| = 14.4°$, and a vertical buckling height $h = 1.49$ Å. The deformation also manifests as a slight asymmetry in the F-F distances within the AgF_4 units (2.947 Å and 2.924 Å). The critical consequence of this complex deformation is that it renders the two Ag sublattices crystallographically inequivalent by removing the inversion center that previously related them.

To establish the origin of AM in AgF_2, we performed a symmetry analysis using `FINDSYM`[30,31] with strict tolerances. The distorted phase is identified as $P2_1$ (No. 4), a non-centrosymmetric polar space group arising from octahedral tilting and buckling of the tetragonal $P4/mmm$ parent. This distortion breaks inversion and fourfold rotational symmetry, leaving a nonsymmorphic screw axis (2_1) as the key operation. The 2_1 symmetry maps the two Ag sublattices onto each other without restoring inversion, thereby fulfilling the defining condition for AM.[6] Crucially, this symmetry reduction enables SOC to generate DM interactions, which are strictly forbidden in centrosymmetric $P4/mmm$, but are essential for stabilizing the topological magnon bands of the altermagnetic state.

The relationship between crystal symmetry and electronic structure is directly reflected in the band dispersions of the two polymorphs [Fig. 1(c)]. In the high-symmetry flat phase, the bands remain fully spin-degenerate throughout the Brillouin zone [Fig. 2(a)], consistent with centrosymmetry and time-reversal symmetry in a conventional, trivial AFM. The system exhibits a direct gap of ∼1.8 eV, with the valence-band maximum at M and the conduction-band minimum at Γ. By contrast, the reduced symmetry of the tilted ground state permits a nonrelativistic, momentum-dependent spin splitting, a defining feature of AM. As shown in Fig. 2(b), this splitting is highly anisotropic: it reaches ∼100 meV along M'–Γ–M,

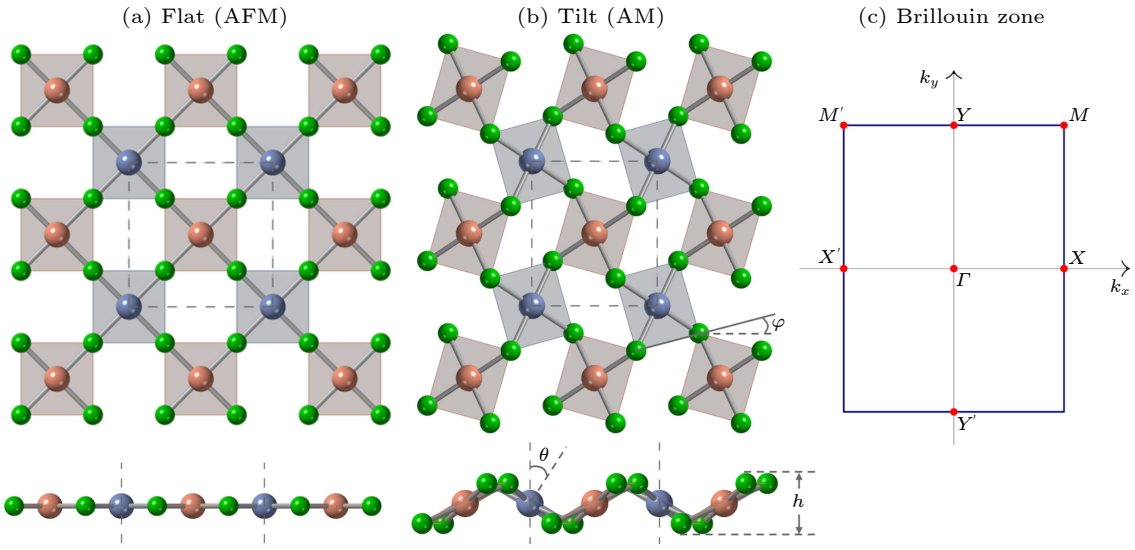

Fig. 1. Structural representations of monolayer AgF_2. Green spheres represent fluorine (F) atoms. Blue and red spheres represent silver (Ag) atoms with opposite magnetic moment projections (positive for blue and negative for red). (a) Flat, high-symmetry reference structure with $a = b$, corresponding to the tetragonal space group $P4/mmm$ (No. 123), used as a non-polar reference phase. (b) Tilted ground-state geometry with characteristic octahedral tilting and polar distortions, belonging to the monoclinic space group $P2_1$ (No. 4). Tilting angles θ, φ, and the vertical displacement h illustrate the broken symmetries. (c) First Brillouin zone of the distorted geometry, with high-symmetry k-points labeled.

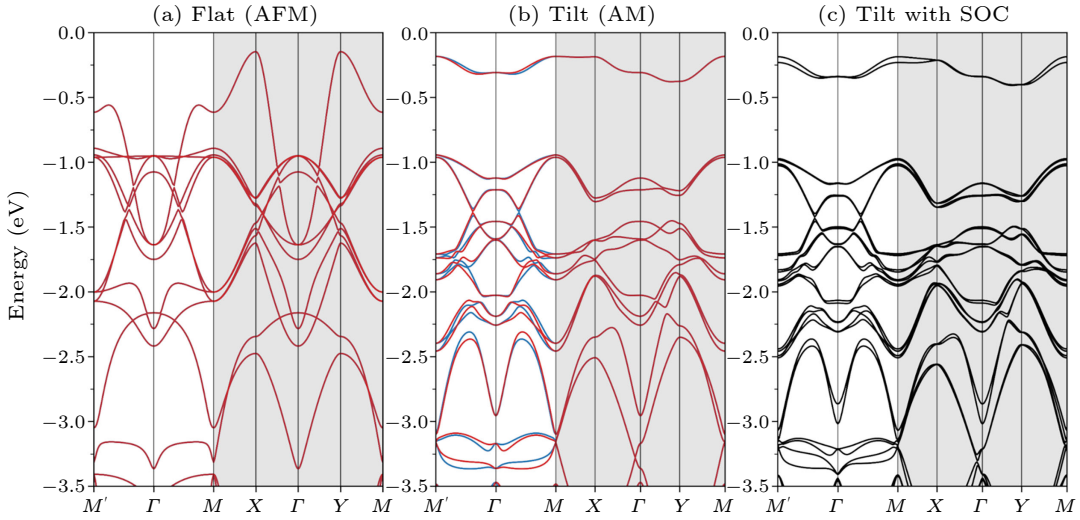

Fig. 2. Electronic band structures of monolayer AgF_2 along the M'–Γ–M–X–Γ–Y–M high-symmetry path. (a) Flat AFM phase, corresponding to the tetragonal space group $P4/mmm$ (No. 123), displays fully spin-degenerate bands. (b) AM ground state with octahedral tilting, belonging to the monoclinic space group $P2_1$ (No. 4), exhibits momentum-dependent spin splitting. Red and blue curves indicate spin-resolved bands within the AM window. (c) AM phase with SOC included, lifting the remaining degeneracies and inducing pronounced splittings at high-symmetry points, particularly near M and M'. Energies are referenced to the Fermi level ($E_F = 0$).

vanishes along Γ–Y, and is strongly suppressed along Γ–X. This pattern reflects the screw symmetry of the $P2_1$ space group: along Γ–Y, the operation $\{C_{2b}|\frac{1}{2}\boldsymbol{b}\}$ preserves local degeneracy, while along generic directions such as M'–Γ–M no such protection exists.[32,33] The resulting exchange-driven, d-wave-like anisotropic spin texture is a hallmark of altermagnetic phases, and originates directly from the symmetry-lowering structural distortion.

3.2. AM+SOC: Electronic Spin–Orbit Effects. The inclusion of relativistic SOC qualitatively enriches the tilted altermagnetic phase of AgF_2. SOC lifts residual degeneracies at symmetry-protected crossings, most notably near the M and M' points, where it opens gaps of up to 20 meV [Fig. 2(c)]. This behavior reflects the absence of inversion and screw symmetries in the $P2_1'$ magnetic space group, consistent with the group-theoretical framework of AM,[6,33] while a detailed symmetry analysis is presented in the Supplementary Materials (SM) together with Refs. [34–36].

Beyond its role in band degeneracies, SOC also determines the magnetic ground state. Our calculations yield a magnetic anisotropy energy of ∼0.2 meV/f.u., favoring

in-plane spins, and a weak ferromagnetic canting that produces a small net moment of $\sim 0.1\,\mu_{\mathrm{B}}$. This canting, symmetry-allowed in the polar $P2_1$ phase and driven by DM interactions,[37] has direct experimental implications: it couples AM order to external magnetic fields, induces nonreciprocal magnon dispersion relevant for magnonic circuits,[8] and provides accessible probes through spin–torque or magneto–optical measurements. Finally, SOC seeds an additional odd-parity p-wave response on top of the dominant d-wave altermagnetic splitting. Such hybridization, absent in the non-relativistic limit, broadens the symmetry-breaking landscape of relativistic altermagnets and enables anisotropic transport phenomena including nonreciprocal conductivity, directional dichroism, and spin-galvanic couplings.[10,38,39]

Quantitatively, we compute the Berry curvature of the top valence bands (Fig. S2 of the SM), revealing large but opposite Chern numbers $C^{\mathrm{E}}_{1,2} = \pm 3$. The vanishing net charge reflects a symmetry-enforced compensation: the anti-unitary operation $(C_{2b}|\frac{1}{2}\boldsymbol{b})\mathcal{T}$ of the magnetic space group $P2'_1$ pairs the two bands into a doublet with exactly cancelling Berry curvatures.[6,8,40,41] Possible routes to lift this compensation and realize a net high-Chern phase ($|C^{\mathrm{E}}| = 3$), as well as the distinction from ferromagnetic and non-collinear antiferromagnetic mechanisms, are discussed in detail in the SM (Sec. SIII-C).[42–51]

3.3. AM+SOC: Symmetry Analysis. To clarify the role of relativistic SOC in the distorted altermagnetic phase of AgF_2, we analyze the magnetic space group symmetry in detail. The tilted $P2_1$ structure lowers the symmetry relative to the tetragonal $P4/mmm$ parent, removing inversion and fourfold rotational symmetry. The relevant magnetic space group is $P2'_1$ (No. 4.9), which contains the anti-unitary operation $(C_{2b}|\frac{1}{2}\boldsymbol{b})\mathcal{T}$: a two-fold screw rotation combined with time reversal. In momentum space, the unitary part C_{2b} acts as $(k_x, k_y, k_z) \mapsto (-k_x, k_y, -k_z)$, while the anti-unitary operation $(C_{2b}|\frac{1}{2}\boldsymbol{b})\mathcal{T}$ maps $\boldsymbol{k} \to -C_{2b}\boldsymbol{k}$ and $\boldsymbol{S} \to -\boldsymbol{S}$. The fractional translation does not alter the star of $\boldsymbol{k}$, but only contributes a phase to the Bloch states. As a result, this symmetry enforces degeneracies only along specific high-symmetry lines such as Γ–Y ($k_x = 0$), where $C_{2b}\boldsymbol{k} \equiv -\boldsymbol{k}$ modulo a reciprocal lattice vector. Away from these lines (e.g., along M'–Γ–M), no such anti-unitary constraint holds, and exchange-driven, even-parity (d-wave-like) altermagnetic splittings are symmetry-allowed.[6]

Moreover, SOC lifts residual degeneracies at zone-boundary points. Most notably, gaps of up to 20 meV open at M and M' [Fig. 2(c)]. Using the `MAXMAGN` tool[34] of the Bilbao Crystallographic Server,[35,36] we find that the little group at $M = (\frac{1}{2}, \frac{1}{2}, 0)$ is the type-I magnetic space group P_s1 (No. 1.3), which lacks anti-unitary operations. In particular, $(C_{2b}|\frac{1}{2}\boldsymbol{b})\mathcal{T}$ does not leave M invariant: under C_{2b}, $(k_x, k_y, k_z) \mapsto (-k_x, k_y, -k_z)$, so $M = (\frac{1}{2}, \frac{1}{2}, 0)$ is mapped to $(-\frac{1}{2}, \frac{1}{2}, 0)$, which is not equivalent to M modulo reciprocal lattice vectors in the monoclinic Brillouin zone. Consequently, this anti-unitary operation does not belong to the little group of M or M'; as a result, no symmetry protects the degeneracy at these points, and SOC is free to open sizable gaps. The M–X segment is highly sensitive to SOC because, in the magnetic space group $P2'_1$ (No. 4.9), this direction is not protected by any symmetry enforcing degeneracy between the two altermagnetic branches. Without SOC, the exchange splitting has a d-wave pattern with nodal lines set by the screw symmetry, and M–X lies close to one of these nodes, strongly suppressing the splitting. SOC introduces an allowed odd-parity p-wave component that hybridizes the nearly degenerate branches and opens a gap. Since the little group at M is P_s1 (No. 1.3), containing no anti-unitary symmetries, the SOC-induced gap becomes particularly pronounced along M–X.

The symmetry reduction of the polar $P2'_1$ phase enables SOC to hybridize the intrinsic even-parity d-wave AM with a subdominant odd-parity p-wave component. Confirmed by multipolar analysis in the SM (Sec. SIII-D[10,39]), this relativistic d/p-wave state is distinct from canonical non-collinear p-wave magnets.[10,11] This unique collinear parity admixture drives anisotropic transport and spin-galvanic couplings,[11,12] effectively underpinning the dual electronic and magnonic topology of AgF_2.

4. Topological Magnons Driven by Altermagnetic Symmetry. In the insulating regime of monolayer AgF_2, charge excitations are suppressed by a large electronic band gap of approximately 1.8 eV. As a result, the low-energy physics is governed by collective spin dynamics, i.e., magnons, rather than electronic quasiparticles. Having established that the structural distortion to the polar $P2_1$ space group breaks global inversion symmetry in the altermagnetic ground state, we now investigate how this reduced symmetry imprints itself on the magnon spectrum. The absence of inversion symmetry enables momentum-dependent spin splitting in the electronic bands, raising the question of whether a similar mechanism leads to a topological magnon phase.

To address this, we construct an effective spin Hamiltonian with isotropic Heisenberg exchange, DM interaction, and symmetric anisotropic exchange parameters extracted from first-principles DFT+U calculations.[25,26,52] Within linear spin-wave theory,[53,54] we compute the magnon modes and analyze their topological character. The magnon band topology is quantified by the integer Chern number (C^{M}), obtained from the Berry curvature of the Bogoliubov–de Gennes eigenvectors[55] using a gauge-invariant numerical scheme.[56] The detailed formalism is provided in the SM.

A nonzero Chern number signals a topological phase, manifested experimentally as a finite transverse thermal Hall conductivity, κ_{xy}.[57,58] In this regime, the Berry curvature acts as an effective magnetic field in momentum space, deflecting magnon flow under a longitudinal temperature gradient and generating a transverse heat current, together with a spin current carried by the magnons, phenomena closely related to the spin Seebeck and spin Nernst effects.[59] Our computed Chern numbers and κ_{xy} therefore predict measurable transverse heat and spin transport in finite AgF_2 samples, establishing thermal Hall measurements as a direct probe of altermagnet-induced magnon topology.[60,61]

4.1. Altermagnons on AgF_2. We now apply the methodology established in the preceding sections to the specific case of monolayer AgF_2. Our analysis demonstrates how the intrinsic altermagnetic symmetry of this material gives rise to a topological magnon phase. A direct comparison between the high-symmetry, flat antiferromagnetic phase and the distorted, tilted altermagnetic state reveals the critical role of symmetry in enabling this phenomenon.

4.1.1. The Topologically Trivial Antiferromagnetic Phase. We analyze the flat, centrosymmetric AFM phase ($P4/mmm$ space group) as the high-symmetry reference for our study. In the absence of SOC, the extracted spin Hamiltonian is purely isotropic and thus exhibits full $SU(2)$ spin-rotation invariance. The spontaneous breaking of this continuous symmetry by the Néel order generates gapless magnon modes at the Γ point, consistent with Goldstone's theorem. Moreover, the $P4/mmm$ symmetry enforces degeneracy of the two magnon modes across the Brillouin zone, as shown in Fig. S3(a) of the SM.

Including SOC does not alter this picture significantly, since the high crystal symmetry largely suppresses relativistic effects. As reported in Table S1 of the SM, the DM interaction, a key ingredient for magnon topology, remains negligible ($|D|/|J_1| \sim 10^{-4}$). SOC does break the $SU(2)$ spin-rotation invariance, lifting the Goldstone protection and opening a small anisotropy gap at Γ [Fig. S3(b) of the SM]. Nevertheless, the Berry curvature remains identically zero throughout the Brillouin zone, confirming that the magnon bands in this phase are topologically trivial.

Beyond these essential features, the AFM magnon spectrum displays a remarkably large bandwidth. The dominant nearest-neighbor coupling, $J_1 \approx -17$ meV, produces a total dispersion exceeding 1.2 eV [Fig. S3(a) of the SM], unusually large for a 2D AFM. In the long-wavelength limit near Γ, the acoustic branch follows the linear dispersion $\hbar\omega(\boldsymbol{k}) \approx v_s|\boldsymbol{k}|$, where the high spin-wave velocity v_s reflects the rigidity of the spin medium. The $P4/mmm$ symmetry also forbids anisotropic interactions, thereby enforcing exact degeneracy of the two branches across the Brillouin zone. While the Mermin–Wagner theorem would preclude long-range order in a strictly isotropic 2D system, the small anisotropy gap induced by SOC [Fig. S3(b) of the SM] is sufficient to stabilize the AFM order. Altogether, these results establish the flat AFM phase as an ideal non-topological baseline for assessing how tilt distortions and SOC drive AgF_2 into an altermagnetic topological magnon phase.

4.1.2. Symmetry-Driven Topology in the Altermagnetic Phase. Unlike the trivial AFM phase, the tilted altermagnetic ground state (polar $P2_1$ space group) provides the symmetry breaking required for non-trivial magnon topology. The structural distortion removes the inversion center and reshapes the magnetic exchange network by weakening J_1, reversing the sign of J_2, and collapsing the magnon bandwidth by more than 60%. As detailed in Table S2 of the SM, all DM interaction terms vanish in the absence of SOC, and the spectrum exhibits gapless Goldstone modes at Γ, confirming that the distortion alone cannot induce a topological phase. Nevertheless, it generates strongly momentum-dependent spin textures and creates ideal conditions for relativistic effects. The resulting magnon modes acquire opposite chirality, directly reflecting the altermagnetic symmetry and establishing the key prerequisite for topology, as confirmed by their spin precession.[7]

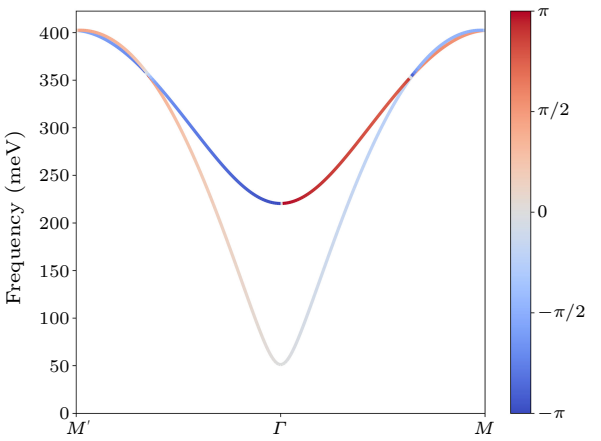

Fig. 3. Chirality of the magnon modes in the AM phase of monolayer AgF_2 including SOC, computed along the high-symmetry path M'–Γ–M. The color scale represents the relative phase angle of magnon precession, $\varphi_s(\boldsymbol{k}) - \varphi_s(\boldsymbol{\Gamma})$, which quantifies the momentum-dependent chirality of the two non-degenerate modes.

When SOC enters, anisotropic interactions dominated by a strong DM interaction give the magnon bands a topological character; the corresponding non-degenerate Tilt + SOC magnon dispersions are shown in Fig. 3. Calculations of the Berry curvature reveal sharp enhancements near the X and Y points, where inter-band gaps narrow and spin textures wind rapidly. Integration over the Brillouin zone yields quantized Chern numbers, $C_1^{\mathrm{M}} = +1$ and $C_2^{\mathrm{M}} = -1$, for the two lowest bands. The finite Berry curvature produces a transverse thermal Hall conductivity (κ_{xy}), a hallmark of topological magnon bands.[57] The low symmetry of the $P2_1$ phase permits this response, and the calculated magnitude matches values reported in pyrochlore and kagome magnets,[58] suggesting that experiments should access it.

The thermal Hall signal (Fig. S5 of the SM) should appear in the low-to-intermediate temperature range below the estimated Néel temperature, $T_{\mathrm{N}} \sim 100$–150 K, where the altermagnetic order and topological bands remain stable. At higher temperatures, magnon–magnon and magnon–phonon scattering will likely reduce the response,[7] but the low-temperature regime firmly establishes the tilted phase of AgF_2 as an altermagnetic topological magnon insulator. Unlike higher-symmetry altermagnets where thermal Hall effects are forbidden, or hematite where topology relies on long-range exchange,[7] AgF_2 derives its topological character from a strong nearest-neighbor DM interaction enabled directly by a polar structural distortion. This mechanism opens a distinct route to robust topological phenomena in collinear, compensated magnets.

4.2. Perspectives. Two-dimensional materials provide a promising platform for multifunctional quantum devices.[62] In this context, the topological chiral magnons predicted here are experimentally accessible through the transverse thermal Hall conductivity, κ_{xy}, which directly probes magnon Berry curvature in collinear magnets without external magnetic fields. For AgF_2 monolayers, a standard Hall-bar geometry should yield a transverse heat current set by the magnon Chern number,[57] with expected $\kappa_{xy} \sim 0.01$–$0.1\,\mathrm{W{\cdot}K^{-1}{\cdot}m^{-1}}$ are anticipated in the low-temperature regime ($T \ll T_\mathrm{N} \sim 100$–$150\,\mathrm{K}$) based on measurements in pyrochlore and kagome AFMs,[58] well within the sensitivity of modern thermal Hall techniques.[61] Complementary momentum-resolved probes such as RIXS, well suited for Ag-based compounds,[63] or in favorable cases inelastic neutron scattering, can directly resolve the nonreciprocal magnon dispersion and the SOC-induced topological gap.

The distortion-driven mechanism that enables chiral topology in AgF_2 is broadly relevant to two-dimensional halides MX_2,[20,21] where polar or ferroelastic octahedral tiltings naturally break inversion symmetry while preserving collinear order.[19] Candidate monolayers include Ag-based fluorides, NiF_2, $CoCl_2$, and MnI_2, which host similar structural instabilities and allow sizable DM interactions once inversion symmetry is removed. The isoelectronic nature of NiF_2 [with a d^8 configuration identical to AgF(II)] makes it especially attractive, while softer halides such as Cl and I may enhance ferroelastic tilting.

From a device perspective, topological chiral magnons support unidirectional, backscattering-immune edge channels,[2,41,55] enabling robust magnonic transport, magnon diodes,[64] and thermally driven logic elements. Combined with electronic readout schemes recently proposed in facet-engineered altermagnetic junctions,[65] our results show that a single material can host both electronic Chern bands ($C^\mathrm{E} = \pm 3$) and magnonic Chern bands ($C^\mathrm{M} = \pm 1$), offering a route to hybrid electron–magnon transduction.[5,8,66] Our findings align with recent predictions of symmetry-driven anomalous transport and Chern-insulating phases in other altermagnets such as CuX_2 (X = F and Cl) and V_2Te_2O,[9,67] highlighting the broader relevance of the dual electronic–magnonic topology uncovered here.

5. Final Remarks. We have demonstrated that monolayer AgF_2 hosts a dual topological phase in its electronic and magnonic excitations, driven by a polar structural distortion to an altermagnetic ground state. By breaking inversion symmetry, this distortion enables SOC to activate a mechanism that simultaneously generates non-relativistic altermagnetic spin splitting and electronic bands carrying large Chern numbers $C^\mathrm{E} = \pm 3$. For the magnons, the same mechanism activates a strong nearest-neighbor DM interaction that opens a topological gap, creating chiral bands characterized by $C^\mathrm{M} = \pm 1$. These magnonic Chern bands yield a finite transverse thermal Hall conductivity and imply the existence of topologically protected edge modes.[41] Although linear spin-wave theory faithfully describes the low-temperature regime, scattering processes at higher temperatures may broaden these signatures.[64] The coexistence of electronic and magnonic topology positions AgF_2 as a prime platform to explore hybrid quantum states, potentially accessible via resonant inelastic x-ray scattering.[63] Conceptually, AgF_2 realizes a relativistic altermagnetic state with a characteristic even/odd-parity (d/p) admixture, which underpins the emergence of both fermionic and bosonic topology. Our findings establish relativistic AM as a natural platform for altermagnonics, where electronic and magnonic topological phases are intrinsically coupled, paving the way for symmetry-engineered quantum devices.

Data Availability. The data that support the findings of this study are available from the corresponding author, upon reasonable request.

Acknowledgements. This work was supported by FONDECYT Regular Grants (Nos. 1250364 and 1250803) and the Basal Program for Centers of Excellence (CEDENNA) (Grant No. CIA250002). Powered@NLHPC: This research was partially supported by the supercomputing infrastructure of the NLHPC (CCSS210001). A.L. acknowledges support from FONDECYT Initiation (Grant No. 11251906).

References

[1] Zhuo F, Kang J, Manchon A, and Cheng Z 2025 *Adv. Phys. Research* **4** 2300054
[2] McClarty P A 2022 *Annu. Rev. Condens. Matter Phys.* **13** 171
[3] Aguilera E, Jaeschke-Ubiergo R, Vidal-Silva N, Torres L E F, and Nunez A 2020 *Phys. Rev. B* **102** 024409
[4] Vidal-Silva N and Troncoso R E 2022 *Phys. Rev. B* **106** 224401
[5] Khatua S, Kravchuk V P, Yershov K V, and van den Brink J 2025 arXiv:2507.17822 [cond-mat.str-el]
[6] Šmejkal L, Sinova J, and Jungwirth T 2022 *Phys. Rev. X* **12** 040501
[7] Hoyer R, Stavropoulos P P, Razpopov A, Valentí R, Šmejkal L, and Mook A 2025 arXiv:2503.11623 [cond-mat.str-el]
[8] Jungwirth T, Fernandes R M, Fradkin E, MacDonald A H, Sinova J, and Šmejkal L 2025 *Newton* **1** 100162
[9] Liu S, Zhang Z, Bai L, and Feng W 2025 *Phys. Rev. B* **111** 184437
[10] Fukaya Y, Lu B, Yada K, Tanaka Y, and Cayao J 2025 *J. Phys.: Condens. Matter* **37** 313003
[11] Hellenes A B, Jungwirth T, Jaeschke-Ubiergo R, Chakraborty A, Sinova J, and Šmejkal L 2023 arXiv:2309.01607 [cond-mat.mes-hall]
[12] Song Q, Stavrić S, Barone P *et al.* 2025 arXiv:2504.21086 [cond-mat.mes-hall]
[13] Sukhachov P, Giil H G, Brekke B, and Linder J 2025 *Phys. Rev. B* **111** L220403
[14] Gawraczyński J, Kurzydłowski D, Ewings R A *et al.* 2019 *Proc. Natl. Acad. Sci. U.S.A.* **116** 1495
[15] Bandaru S, Derzsi M, Grzelak A, Lorenzana J, and Grochala W 2021 *Phys. Rev. Materials* **5** 064801
[16] Liu X, Pandey S K, and Feng J 2022 *Phys. Rev. B* **105** 134519
[17] Grzelak A, Derzsi M, and Grochala W 2021 *Inorg. Chem.* **60** 1561
[18] Hong S, Park M J, and Kim K M 2025 *Phys. Rev. B* **111** 054501
[19] Peng R, Fang S, Ho P, Zhou T, Liu J W, and Ang Y S 2025 arXiv:2505.20843 [cond-mat.mtrl-sci]

[20] Botana A S and Norman M R 2019 *Phys. Rev. Materials* **3** 044001
[21] Fukuda M, Zhang J, Lee Y T, and Ozaki T 2021 *Mater. Adv.* **2** 4392
[22] Kresse G and Hafner J 1993 *Phys. Rev. B* **47** 558
[23] Kresse G and Joubert D 1999 *Phys. Rev. B* **59** 1758
[24] Perdew J P, Burke K, and Ernzerhof M 1996 *Phys. Rev. Lett.* **77** 3865
[25] Ozaki T and Kino H 2004 *Phys. Rev. B* **69** 195113
[26] Ozaki T and Kino H 2005 *Physi. Rev. B* **72** 045121
[27] Monkhorst H J and Pack J D 1976 *Phys. Rev. B* **13** 5188
[28] Dudarev S L, Botton G A, Savrasov S Y, Humphreys C, and Sutton A P 1998 *Phys. Rev. B* **57** 1505
[29] Domański M A, Derzsi M, and Grochala W 2021 *RSC Adv.* **11** 25801
[30] Stokes H T and Hatch D M 2005 *J. Appl. Cryst.* **38** 237
[31] Stokes H T, Hatch D M, and Campbell B J 2025 FINDSYM (Version 7.1.7) [Software]
[32] Qayyum H A, Mansha M, and Sattar S 2024 *ACS omega* **9** 47097
[33] Sheoran S and Bhattacharya S 2024 *Phys. Rev. Mater.* **8** L051401
[34] Bilbao Crystallographic Server, MAXMAGN: Maximal magnetic space groups
[35] Aroyo M I, Perez-Mato J M, Capillas C, Kroumova E, Ivantchev S, Madariaga G, Kirov A, and Wondratschek H 2006 *Z. Kristallogr. - Cryst. Mater.* **221** 15
[36] Perez-Mato J, Gallego S, Tasci E, Elcoro L, de la Flor G, and Aroyo M 2015 *Annu. Rev. Mater. Res.* **45** 217
[37] Moriya T 1960 *Phys. Rev.* **120** 91
[38] Wang S, Wang W W, Fan J, Zhou X, Li X P, and Wang L 2025 arXiv:2504.19585 [cond-mat.mtrl-sci]
[39] León A, Autieri C, Brumme T, and González J W 2025 *npj Quantum Mater.* **10** 98
[40] Armitage N P, Mele E J, and Vishwanath A 2018 *Rev. Mod. Phys.* **90** 015001
[41] Hatsugai Y 1993 *Phys. Rev. Lett.* **71** 3697
[42] González J W, León A M, González-Fuentes C, and Gallardo R A 2025 *Nanoscale* **17** 4796
[43] Huang A, Ke S, Guan J H, Li J, and Lou W K 2024 *Phys. Rev. B* **109** 045408
[44] You J Y, Dong X J, Gu B, and Su G 2021 *Phys. Rev. B* **103** 104403
[45] Chen H, Lu J, Wang N, Zhao X, Hu G, Yuan X, and Ren J 2024 *Appl. Phys. Lett.* **124** 153101
[46] Bao K, Wang H, Guo J, Jiang Y, Xu H, and Wang J 2025 *Phys. Rev. B* **111** 205135
[47] Hadad Y, Khanikaev A B, and Alu A 2016 *Phys. Rev. B* **93** 155112
[48] Lian H, Xu X, Lu J, Rui X, Qi L, Yao X, He A, and Zhang X 2025 *Adv. Quantum Technol.* **8** 2400444
[49] Li S, Li X, Ji W, Li P, Yan S, and Zhang C 2023 *Phys. Chem. Chem. Phys.* **25** 18275
[50] Chen P, Zou J Y, and Liu B G 2017 *Phys. Chem. Chem. Phys.* **19** 13432
[51] Lian B, Liu Z, Zhang Y, and Wang J 2020 *Phys. Rev. Lett.* **124** 126402
[52] He X, Helbig N, Verstraete M J, and Bousquet E 2021 *Comput. Phys. Commun.* **264** 107938
[53] Rybakov A 2026 MAGNOPY (v0.4.3) [Computer software and documentation]
[54] Ivanov A V, Uzdin V M, and Jónsson H 2021 *Comput. Phys. Commun.* **260** 107749
[55] Shindou R, Matsumoto R, Murakami S, and Ohe J I 2013 *Phys. Rev. B* **87** 174427
[56] Fukui T, Hatsugai Y, and Suzuki H 2005 *J. Phys. Soc. Jpn.* **74** 1674
[57] Katsura H, Nagaosa N, and Lee P A 2010 *Phys. Rev. Lett.* **104** 066403
[58] Onose Y, Ideue T, Katsura H, Shiomi Y, Nagaosa N, and Tokura Y 2010 *Science* **329** 297
[59] Uchida K I, Takahashi S, Harii K, Ieda J, Koshibae W, Ando K, Maekawa S, and Saitoh E 2008 *Nature* **455** 778
[60] Nagaosa N and Tokura Y 2013 *Nat. Nanotech.* **8** 899
[61] Uchida K, Ishida M, Kikkawa T, Kirihara A, Murakami T, and Saitoh E 2014 *J. Phys.: Condens. Matter* **26** 343202
[62] Wang Z, Wang M, Heine T, and Feng X 2025 *Nat. Rev. Mater.* **10** 147
[63] Li J, Gu Y, Takahashi Y *et al.* 2023 *Phys. Rev. X* **13** 011012
[64] Mook A, Plekhanov K, Klinovaja J, and Loss D 2021 *Phys. Rev. X* **11** 021061
[65] Chi B, Jiang L, Zhu Y, Yu G, Wan C, Zhang J, and Han X 2024 *Phys. Rev. Appl.* **21** 034038
[66] Zhang M H, Xiao L, and Yao D X 2024 arXiv:2407.18379 [cond-mat.mes-hall]
[67] Wang Z, Wu R, Ma C, Gong S, Zhao C, Zhang S, Wang G, Wang T, and An Y 2025 *Chin. Phys. Lett.* **42** 080705